Inorganic Chemistry

Article

pubs.acs.org/IC

Continuous Control of Optical Gaps in Quasi-One-Dimensional Bromide-Bridged Platinum Complexes by Utilizing Chemical Pressure

Shohei Kumagai,[†,‡] Hiroaki Iguchi,[†] Shinya Takaishi,*[,†] Brian K. Breedlove,[†] Masahiro Yamashita,*[,†,‡,§] Hiroyuki Matsuzaki,[∥,∇] Hiroshi Okamoto,[∥] Kenichi Kato,[⊥,#] and Masaki Takata[#,⊥]

[†]Department of Chemistry, Graduate School of Science, Tohoku University, 6-3 Aza-Aoba, Aramaki, Aoba-ku, Sendai, Miyagi 980-8578, Japan

[‡]WPI-Advanced Institute for Materials Research, Tohoku University, 2-1-1 Katahira, Aoba-ku, Sendai, Miyagi 980-8577, Japan

[§]CREST, JST, 4-1-8 Honcho, Kawaguchi, Saitama 332-0012, Japan

[∥]Department of Advanced Material Science, Graduate School of Frontier Sciences, The University of Tokyo, Kashiwa, Chiba 277-8561, Japan

[⊥]RIKEN SPring-8 Center, Sayo-gun, Hyogo 679-5148, Japan

[#]Japan Synchrotron Radiation Research Institute, Sayo-gun, Hyogo 679-5198, Japan

Supporting Information

ABSTRACT: The optical gap in a series of bromo-bridged platinum chain complexes, $[Pt(en)_2Br](C_n{-}Y)_2{\cdot}H_2O$ (en = ethylenediamine; C_n−Y = dialkyl sulfosuccinate; n = the number of carbon atoms), was controlled by using chemical pressure. From the single-crystal structure, $[Pt(en)_2Br](C_6{-}Y)_2{\cdot}H_2O$ is in a mixed-valence state at 200 K. In addition, Pt−Pt distances decreased with an increase in n or with a decrease in the temperature. Continuous decreases in the optical gaps upon cooling were observed for n = 5, 7. The smallest gap of 1.20 eV was observed for n = 7 at 50 K. For n = 12, the complex was still in a mixed-valence state at 5 K, although the Pt−Pt distance was quite short. This is probably because of the energetic mismatch between $5d_{z^2}$ orbitals of the Pt ions and $4p_z$ orbitals of the Br ions.

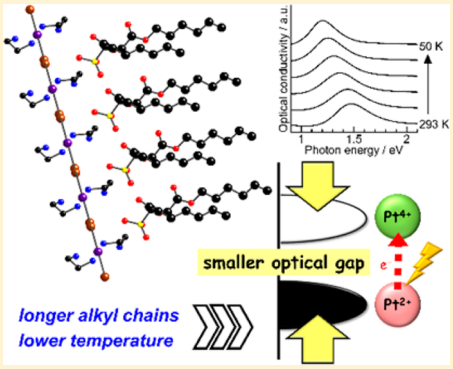

INTRODUCTION

Quasi-one-dimensional (1D) halogen-bridged metal complexes (MX chains), such as Wolffram's red salt analogues, exhibit several characteristic chemical and physical properties, such as intense and dichroic charge transfer (CT) bands,[1] progressive overtones in the resonance Raman spectra,[2] midgap absorptions attributable to solitons and polarons,[3] gigantic third-order nonlinear optical susceptibilities,[4] and spin−Peierls transitions.[5] They have 1D linear chain structures in which the d_{z^2} orbitals of the metal (M) ions and the p_z orbitals of the bridging halide (X) ions overlap along the chain (represented as −M−X−M−X−) and, thus, have highly isolated 1D electron systems. MX chains are extended Peierls−Hubbard systems, where the electron−lattice interaction (S), the transfer integral (t), and the on-site and nearest-neighbor Coulomb repulsion energies (U and V, respectively) strongly compete with each other.[6] As a result, the electronic states are coupled with the lattice distortion. In other words, if the X ions are located at the midpoint between the neighboring M ions, the 1D chain is represented as $-X-M^{III}-X-M^{III}-X-$, which is called averaged valence (AV) state. This state occurs due to large U values of the M ions ($U > S$),[7] which means that Ni MX chains are usually in AV states. In addition, these types of Ni MX chains are Robin−Day class III complexes.[8]

On the other hand, Pt and Pd MX chains easily form M(II)−M(IV) mixed-valence (MV) states where the X ions are displaced from the midpoints between the M ions, represented as $-X\cdots M^{II}\cdots X-M^{IV}-X\cdots$, as a consequence of large S values ($S > U$). These Pt and Pd MX chains are classified as Robin−Day class II mixed-valence complexes.[8] However, the valences are actually $+(3 \pm \delta)$, where δ is the degree of the charge disproportionation ($0 \le \delta \le 1$). The value of δ is closely related to the M−M distance (L) and the resultant displacement of the X ions.[9] Although more than 300 complexes have been synthesized since Wolffram reported the first mixed-valence salt $[Pt^{II}(NH_2C_2H_5)_4][Pt^{IV}Cl_2(NH_2C_2H_5)_4]Cl_4{\cdot}4H_2O$ in 1900,[10] before our research, Pt and Pd MX chains had been found to be only in the MV states and Ni MX chains were only in AV states.[11]

Okamoto et al. have investigated the relationship between the electronic state and the features of the 1D chain structure in

Received: August 27, 2014
Published: October 23, 2014

 © 2014 American Chemical Society dx.doi.org/10.1021/ic502071u | Inorg. Chem. 2014, 53, 11764−11769

a series of MX chains.[9] Figure 1 shows the M−X distance as a function of L for different complexes.[9] The short and long M−X distances (l_1 and l_2, respectively) are assigned to M^{IV}−X and M^{II}−X units, respectively. As can be seen, X ions approach the midpoint, i.e., the difference between l_1 and l_2 becomes small, as L decreases, indicating that the compounds approach AV states when L becomes small. On the basis of this feature, we have recently prepared a Pd(III) chain in an AV state by applying chemical pressure between alkyl chains in the countercations to shorten L.[11] This result motivated us to adopt the same strategy to prepare the first Pt(III) AV state. In the present work, we synthesized Br-bridged Pt complexes with long alkyl chains in the countercations used to prepare the Pd(III) chains. In this paper, we report the relationship between the structural and optical properties of $[Pt(en)_2Br](C_n{-}Y)_2{\cdot}H_2O$ (C_n−Y = dialkyl sulfosuccinate; n = 5, 6, 7, 9, 12).

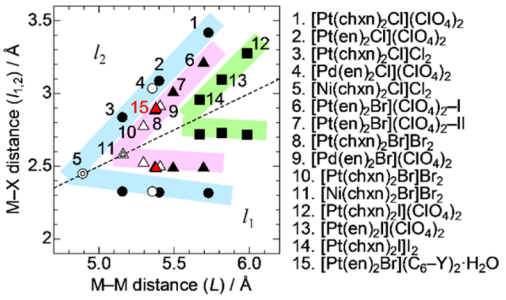

Figure 1. Correlation between M−X distances $l_{1,2}$ and M−M distance L. Circles, triangles, and squares represent the Cl-, Br-, and I-bridged MX chains, respectively. Filled, hollow, and double markers show Pt, Pd, and Ni MX chains, respectively. Blue, pink, and green highlight lines are guides for the eyes for each X ion. The data, except for entry 15, are taken from ref 9.

EXPERIMENTAL SECTION

Materials. All chemicals and solvents were purchased from Wako, TCI, Aldrich, and Soekawa Chemical Co. Ltd. (Japan) and used without further purification.

X-ray Crystal Structure Analyses. Single-crystal X-ray data were acquired on a Bruker SMART APEX CCD diffractometer with graphite-monochromated Mo Kα radiation (λ = 0.7107 Å). Powder X-ray diffraction patterns were measured by using a Debye−Scherrer camera in the beamline 02B2[12] and synchrotron X-ray source (λ = 1.0828 Å) installed at SPring-8. Lattice parameters were refined using the LeBail method.[13]

Polarized Fourier Transform Infrared Spectroscopy. Polarized Fourier transform infrared (FT-IR) spectra were measured on a JASCO FT/IR-6200YMS instrument with a JASCO ITR-5000 infrared microscope.

Polarized Reflectivity Spectroscopy. Polarized reflectivity spectra were obtained by using a specially designed spectrometer with a 25 cm grating monochromator and an optical microscope. Optical conductivity spectra were obtained by using the Kramers−Krönig transformation on the reflectivity spectra.[14]

Polarized Raman Spectroscopy. Polarized Raman spectra were acquired on a Renishaw Raman spectrometer. A He−Ne laser (λ = 632.8 nm) was used for excitation.

Ultraviolet−Visible-Near-Infrared Spectroscopy. Ultraviolet−visible-near-infrared (UV−vis−NIR) spectra were acquired on a Shimadzu UV-3100 instrument. Measurements were carried out at room temperature (T).

Spin Coating. A Mikasa 1H-D7 spin coater was used for fabricating thin films.

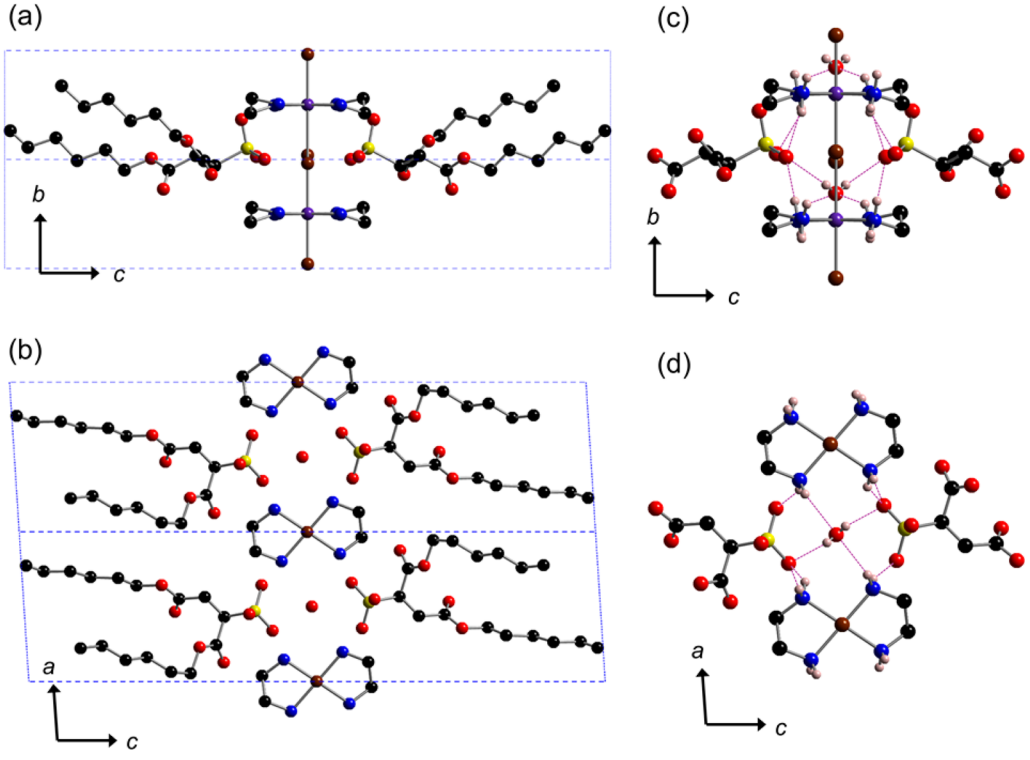

Figure 2. (a, b) Crystal structure of $[Pt(en)_2Br](C_6{-}Y)_2{\cdot}H_2O$ viewed from (a) the a axis and (b) the b axis. Hydrogen atoms are omitted for clarity. In (a), water molecules are omitted for clarity. Color code: purple, Pt; brown, Br; black, C; blue, N; red, O; yellow, S. (c, d) Hydrogen-bond network formed among en ligands, sulfonate ions and crystal waters viewed from (c) the a axis and (b) the b axis. Violet dotted lines represent the hydrogen bonds. Alkyl-chain moieties and H atoms bound to C atoms are omitted for clarity.

dx.doi.org/10.1021/ic502071u | Inorg. Chem. 2014, 53, 11764−11769

Preparation of Starting Materials. Sodium salts of the counterions Na(C_n−Y) (n = 5, 6, 7, 9, 12)[11] and single crystals of [Pt(chxn)$_2$Br]Br$_2$ (chxn = 1*R*,2*R*-diaminocyclohexane)[15] were synthesized following previously reported methods.

Preparation of Single Crystals of Pt Complexes. Single crystals of [Pt(en)$_2$Br](C_n−Y)$_2$·H$_2$O were prepared by slow diffusion of an aqueous mixture of [Pt(en)$_2$]Br$_2$ and [Pt(en)$_2$Br$_2$]Br$_2$ and a tetrahydrofuran solution of Na(C_n−Y). Single crystals of [Pt(en)$_2$Br]-(C_n−Y)$_2$·H$_2$O were obtained as red-brown (n = 5−7) and blue thin plate-shaped crystals (n = 9, 12).

Preparation of Thin Films. [Pt(en)$_2$Br](C_n−Y)$_2$·H$_2$O (5 mg) was suspended in CH$_2$Cl$_2$ or CH$_2$Cl$_2$/toluene (1/3 (v/v); 0.9 mL). To the suspension was added poly(methyl methacrylate) (PMMA; 40 mg), and then the suspension was placed in ultrasonifier for 5 min. The resulting solution was filtered through a glass syringe filter with a pore diameter of 1.0 μm. The filtrate was stored in the refrigerator for several hours and then casted onto the transparent SiO$_2$ substrate rotating at 5500 rpm, affording the thin films used in the UV−vis−NIR measurements.

RESULTS AND DISCUSSION

Structural Characterization. The crystal structure and crystal data of [Pt(en)$_2$Br](C_6−Y)$_2$·H$_2$O (represented as n = 6) at 200 K are shown in Figure 2 and summarized in Table 1,

Table 1. Crystal Data for [Pt(en)$_2$Br](C_6−Y)$_2$·H$_2$O

formula	$C_{36}H_{76}BrN_4O_{15}PtS_2$
formula mass (amu)	1144.13
space group	*P*2
cryst syst	monoclinic
CCDC no.	1016556
cryst size (mm^3)	0.50 × 0.20 × 0.02
a (Å)	7.793(4)
b (Å)	5.379(3)
c (Å)	29.962(15)
β (deg)	93.680(7)
V (Å^3)	1253.4(11)
Z	1
T (K)	200(2)
μ (mm^{-1})	3.741
ρ_{calcd} (g cm^{-3})	1.516
F(000)	585
GOF on F^2	1.035
R1, wR2 ($I > 2\sigma(I)$)	0.0341, 0.0825
R1, wR2 (all data)	0.0347, 0.0829
no. of rflns measd	4275
Flack param	0.211(9)
θ range for data collection (deg)	2.04−25.90
R_{int}	0.0293

respectively. As shown in Figure 2, Pt(en)$_2$ moieties are bridged by Br ions, forming a 1D chain. The chain structure is stabilized by the two-dimensional hydrogen-bond networks within the *ab* plane, composed of N−H···O hydrogen bonds between the N−H hydrogen of the en ligands and the O atom of sulfonate groups, between the N−H hydrogen of the en ligands and the O atom of the water molecules, and O−H···O hydrogen bonds between the hydrogen of the water molecules and the O atom of sulfonate groups. Those are shown as broken lines in Figure 2c,d. Although we used a racemic mixture of Na(C_6−Y) as the starting material, the crystals used for an X-ray crystal structure analysis preferentially contained the *R* form of the C_6−Y$^-$ group. In other words, [Pt(en)$_2$Br](C_6−Y)$_2$·H$_2$O spontaneously crystallized in enanttiopure form. [Pt(en)$_2$Br](C_6−Y)$_2$·H$_2$O is isostructural with [Pd(en)$_2$Br](C_5−Y)$_2$·H$_2$O.[11] The bridging Br ions are disordered and displaced from the midpoint between two neighboring Pt ions, indicating that this MX chain is in an MV state.

As shown in Table 2, there are short (2.484 ± 0.002 Å) and long Pt−Br bond lengths (2.895 ± 0.03 Å). Because the Pt^{II}−Br distances should be longer than the Pt^{IV}−Br distances, the former and latter bonds are assigned to Pt^{IV}−Br and Pt^{II}−Br, respectively. In Figure 1, we plotted the M−X distances for n = 6 (red triangles). They fell on the line for Br-bridged MX chains (bold pink line covering the triangles). In addition, it has been established that the displacement parameter (d), which is defined by $d = (l_2 - l_1)/(l_2 + l_1)$, highly depends on L ($\equiv l_1 + l_2$). We plotted the correlation between d and L for several MX chains (Figure 3). The value of d for n = 6 at 200 K (d = 0.0764) obeys the correlation. Thus, the electronic states of the present compounds could be systematically compared with those of the other Br-bridged MX chains.

Table 2. Selected Bond Lengths (Å) and Angles (deg) for [Pt(en)$_2$Br](C_6−Y)$_2$·H$_2$O at 200 K

	bond length (Å) or bond angle (deg)
Pt−N	2.042(4), 2.050(4)
Pt(1)−Br(1)	2.486(5), 2.893(5)
Pt(1)−Br(2)	2.482(7), 2.898(7)
N−Pt−N (neighbor)	82.83(17), 97.19(17)
N−Pt−N (diagonal)	178.5(7), 178.6(6)
Br−Pt−Br	180.000(3)

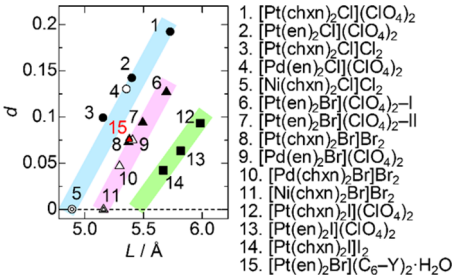

Figure 3. Correlation between parameters d and L. Circles, triangles, and squares represent the Cl-, Br-, and I-bridged MX chains, respectively. Filled, hollow, and double markers represent the Pt, Pd, and Ni MX chains, respectively. Blue, pink, and green highlight lines are guides for the eyes for each X ion. The data, except for entry 15, are taken from ref 9.

The T dependences of L, which were determined by LeBail fitting[13] of the powder X-ray diffraction (PXRD) patterns for [Pt(en)$_2$Br](C_n−Y)$_2$·H$_2$O (n = 5, 6, 7, 9, 12), are shown in Figure 4a. For all MX chains, L continuously decreased with a decrease in T. The L values of both n = 5 and n = 6 at 300 K were approximately 5.39 Å. This is slightly longer than that of [Pt(chxn)$_2$Br]Br$_2$ (5.37 Å),[15] which has the shortest Pt−Pt distance among known Br-bridged Pt chains and is in an MV state. Upon cooling, L of n = 5 and n = 6 decreased to 5.32 Å (or by ca. 1.5%) at 90 K, whereas that of [Pt(chxn)$_2$Br]Br$_2$ showed almost no T dependence (crosses in Figure 4a). The large T dependences in the present complexes are thought to be due to the suppression of the thermal motion of the alkyl chains.[11] In terms of the n dependence of L, longer alkyl chains caused the L value to decrease even at room T (Figure 4b).

dx.doi.org/10.1021/ic502071u | *Inorg. Chem.* 2014, 53, 11764−11769

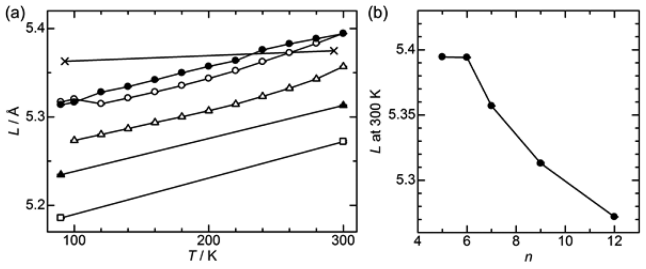

Figure 4. (a) T dependences of L for $[Pt(en)_2Br](C_n{-}Y)_2{\cdot}H_2O$ (hollow circle, n = 5; filled circle, n = 6; hollow triangle, n = 7; filled triangle, n = 9; hollow square, n = 12) and $[Pt(chxn)_2Br]Br_2$ (cross). (b) n dependence of L at 300 K.

This finding is same as that for the Br-bridged Pd MX chains. L in $[Pt(en)_2Br](C_n{-}Y)_2{\cdot}H_2O$ was shorter than that in $[Pt(chxn)_2Br]Br_2$ at room T when $n \geq 9$. It should be noted that the L value of 5.18 Å (n = 12 at 90 K) is shorter than the boundary distance (5.26 Å) between MV and AV states observed for $[Pd(en)_2Br](C_5{-}Y)_2{\cdot}H_2O$.[11] Thus, we investigated the electronic state because it was thought that the n = 12 MX chain would be in an AV state at 90 K. Because it is difficult to confirm the electronic state solely from PXRD analysis, the optical properties were investigated.

Optical Absorption Spectra. We determined the n dependence of the optical gap (E_g) at room T. It is known that a short L value or a small d value indicates a small E_g value for MX chains.[9] In the present work, E_g values were estimated from the UV–vis–NIR absorption spectra for KBr pellets and thin films of $[Pt(en)_2Br](C_n{-}Y)_2{\cdot}H_2O$ ($6 \leq n \leq 12$). Kimizuka et al. have reported that nanocrystalline $[Pt(en)_2Cl](C_n{-}Y)_2{\cdot}H_2O$ can be dispersed in appropriate organic media.[16] In the present study, a suspension of the nanocrystals of the MX chains in PMMA matrix were deposited onto a SiO_2 substrate to form thin films. The spectra for KBr pellets and thin films are shown in Figure 5a, respectively. In all spectra, a broad

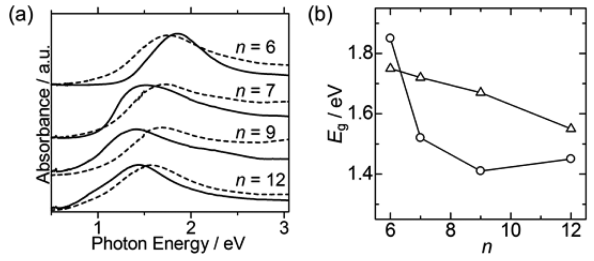

Figure 5. (a) UV–vis–NIR absorption spectra for KBr pellets (broken lines) and thin films (solid lines) of $[Pt(en)_2Br](C_n{-}Y)_2{\cdot}H_2O$ at room T. (b) n dependence of E_g at room T for $[Pt(en)_2Br](C_n{-}Y)_2{\cdot}H_2O$: triangle, KBr pellets; circle, thin films.

absorption band was observed in the energy range measured for each complex. This broad absorption band is thought to be due to intervalence charge transfer from the Pt^{II} to Pt^{IV} ions. Thus, the peak top was used as E_g. The E_g values are plotted as a function of n in Figure 5b. At room T, E_g continuously decreased with an increase in n, which was observed for both measurement methods. This trend is consistent with the n dependence of L shown in Figure 4b. However, E_g values estimated from KBr pellets are relatively larger than those from thin films. This is probably due to the contribution of diffuse reflection of the incident light, which is dominant when the particle size is larger than the wavelengths of the lights. In the case of polymer blended thin films, on the other hand, we used a 1.0 μm diameter glass filter before spin coating, which minimized the diffuse reflectance contribution. Thus, E_g values estimated from thin film data should be more accurate than those from KBr pellet data.

Optical conductivity spectra for $[Pt(en)_2Br](C_n{-}Y)_2{\cdot}H_2O$, which were obtained by using the Kramers–Krönig transformation of specular reflectivity spectra[14] for single crystals, were acquired to determine whether the E_g values acquired from the absorption spectra for the thin films were reasonable. In Figure 6, the T dependence of the optical conductivity

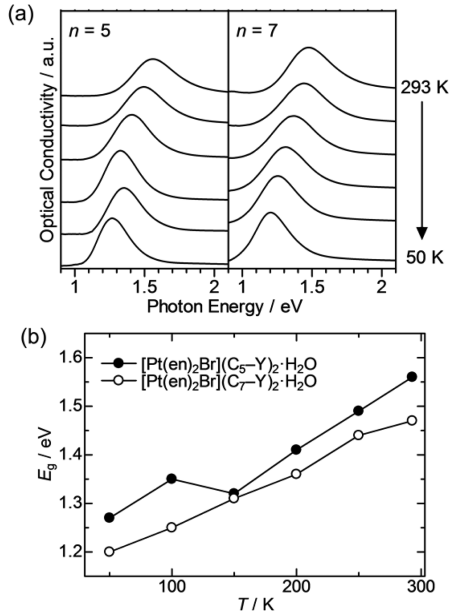

Figure 6. (a) T dependence of optical conductivity spectra for $[Pt(en)_2Br](C_n{-}Y)_2{\cdot}H_2O$ with n = 5 (left panel) and 7 (right panel). (b) T dependence of E_g determined from (a).

spectra and E_g for n = 5, 7 are shown. From the plots, it is clear that the estimated E_g values for thin films (1.52 eV) and the single crystals (1.47 eV) are similar in the n = 7 MX chain. The structural difference between nanocrystal and bulk, therefore, is considered to be small. Moreover, as seen in Figure 4a, the E_g values decreased with a decrease in T. The E_g of 1.20 eV for n = 7 at 50 K is the smallest value among the Br-bridged Pt chains reported so far. As mentioned above, the results show that suppression of the thermal motion of alkyl chains in the countercations causes a decrease in L. We could not obtain the optical conductivity spectra and the E_g values for $n \geq 9$ because the crystals were not large enough.

Raman Spectra. Raman spectroscopy is a powerful tool for studying the electronic states of MX chains. It is well-known that MX chains in MV states, such as the Pt complexes, show Raman peaks characteristic of $X{-}M^{IV}{-}X$ symmetrical stretching modes. On the other hand, those in AV states do not show such Raman signals because the $X{-}M^{III}{-}X$ symmetrical stretching mode is forbidden. We acquired polarized Raman spectra for the n = 12 MX chain in the range 10–300 K (Figure 7). Over the entire T range, intense and relatively weak bands were observed near 175 cm^{-1} (ν_1) and 350 cm^{-1} (ν_2), respectively. They were assigned to the normal and the second-harmonic vibrations of $Br{-}Pt^{IV}{-}Br$ symmetrical stretching

dx.doi.org/10.1021/ic502071u | Inorg. Chem. 2014, 53, 11764–11769

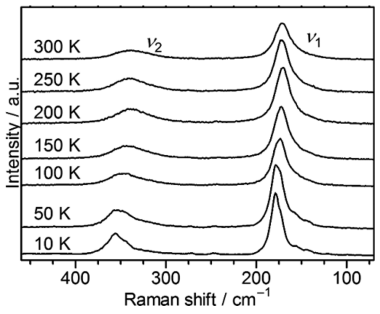

Figure 7. Polarized Raman spectra for $[Pt(en)_2Br](C_{12}–Y)_2·H_2O$ in the range 10–300 K. Polarization ($\boldsymbol{E}$) is parallel to the b axis ($\boldsymbol{E}\|\boldsymbol{b}$).

modes, respectively. These bands were observed even at 10 K, indicating that the n = 12 MX chain was still in an MV state even at 10 K.

FT-IR Spectra. For more information on the electronic state of the n = 12 MX chain, polarized FT-IR spectra were acquired because the N–H symmetrical stretching energies of the in-plane ligands would be different depending on the charge state of the M ions to which they are coordinated.[17] As can be seen in spectra for the n = 6 MX chain in the left panel of Figure 8a,

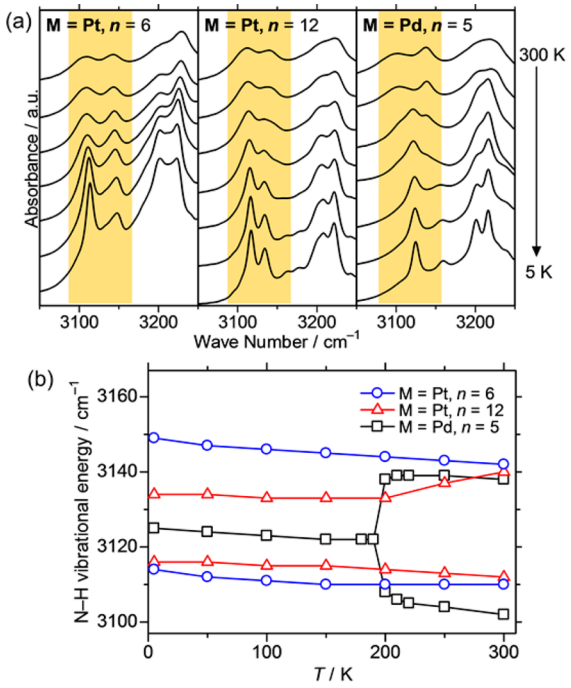

Figure 8. (a) Polarized FT-IR spectra for $[M(en)_2Br](C_n–Y)_2·H_2O$ in the range 5–300 K: $\boldsymbol{E}\perp\boldsymbol{b}$. Regions shaded in yellow are assigned to the N–H symmetrical vibrations. (b) T dependence of N–H symmetrical vibrational energy.

two peaks were observed in the range 3100–3150 cm^{-1} over the entire T range studied. These were assigned to the N–H symmetrical stretching of amino groups coordinated to the $Pt^{II/IV}$ ions. On the other hand, the spectra for $[Pd(en)_2Br](C_5–Y)_2·H_2O$, which has been reported to show an MV-to-AV phase transition at 206 ± 2 K[11] and thus was used as a reference in this study, clearly changed (the right panel of Figure 8a). A single peak for the N–H stretching mode implied that $[Pd(en)_2Br](C_5–Y)_2·H_2O$ was in an AV state at low T. Therefore, we concluded that the n = 6 MX chain was in an MV state at 5 K. Like the spectra for the n = 6 MX chain, those for the n = 12 MX chain (the central panel of Figure 8a) indicated that the n = 12 MX chain was also in an MV state at 5 K.

Comparison with Pd MX Chains. Finally, the n = 12 MX chain is not in an AV state, in spite of having a shorter L value than those of the Pd MX chains in AV states. A correlation between L and E_g for $[M(en)_2Br](C_5–Y)_2·H_2O$ (M = Pd, Pt) in MV states is plotted in Figure 9. Although the ionic radii of

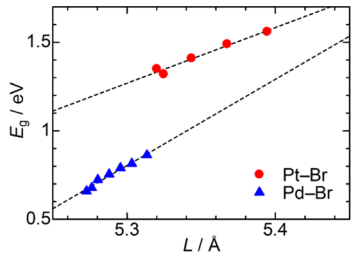

Figure 9. Correlation between E_g and L in $[M(en)_2Br](C_5–Y)_2·H_2O$ (M = Pd, Pt): red circle, M = Pt; blue triangle, M = Pd. The dashed lines are guides for the eyes.

the Pd and Pt ions are similar[18] and the counterions used are the same, the Pt complex has an E_g value much larger than that for the Pd complex. In particular, when the L values in both MX chains were ca. 5.32 Å, the difference in E_g values was ca. 0.4 eV. We think this is because the valence orbitals used for the construction of the 1D chains are different. The energy of the $4p_z$ orbital of the Br ions is far from that of the $5d_{z^2}$ orbital of the Pt ions in comparison to that for the $4d_{z^2}$ orbital of the Pd ions, resulting in the relatively higher ionic nature of the Pt–Br bonds. Moreover, a large t value makes the valence and conduction bands wider, resulting in a smaller E_g. Since t becomes larger as the covalency of the M–X bond increases, the bandwidth in the Pd–Br chains should be larger than that in the Pt–Br chains. Therefore, the Pt MX chains have a large E_g value. Since the MV state is stabilized when t is small, we did not observe a phase transition for $[Pt(en)_2Br](C_{12}–Y)_2·H_2O$, although L was shorter than that in the Pd MX chains.

CONCLUSIONS

We synthesized Br-bridged Pt chain complexes, $[Pt(en)_2Br](C_n–Y)_2·H_2O$ (n = 5, 6, 7, 9, 12), and found that $[Pt(en)_2Br](C_6–Y)_2·H_2O$ was in an MV state at 200 K by using a single-crystal structure determination. PXRD analyses showed that increasing n and lowering T caused the Pt–Pt distances to decrease. For $[Pt(en)_2Br](C_{12}–Y)_2·H_2O$, the Pt–Pt distance was calculated to be 5.18 Å at 90 K, which is the shortest value among the Br-bridged Pt chains reported so far. In addition, E_g decreased with an increase in n and a decrease in T. The smallest E_g value of 1.20 eV was observed for $[Pt(en)_2Br](C_7–Y)_2·H_2O$ at 50 K. $[Pt(en)_2Br](C_{12}–Y)_2·H_2O$ should have the smallest E_g value due to its short L value. However, we could not determine its value in the present study. FT-IR spectra indicated that $[Pt(en)_2Br](C_{12}–Y)_2·H_2O$ was in an MV state even at 5 K, although the Pt–Pt distance was quite short. We think that this is due to the relationship between the energy levels of the $5d_{z^2}$ orbitals of the Pt ions and $4p_z$ orbitals of the Br ions, which is critical for the phase transition to occur. We are currently preparing I-bridged Pt chains because, as our results show, they are better candidates for realizing a Pt(III) AV state.

dx.doi.org/10.1021/ic502071u | Inorg. Chem. 2014, 53, 11764–11769

■ ASSOCIATED CONTENT

Supporting Information

Figures, a table, and a CIF file giving the results of LeBail fitting on powder X-ray diffraction patterns, reflectivity spectra, and crystallographic data. This material is available free of charge via the Internet at http://pubs.acs.org. Crystallographic data have also been deposited with The Cambridge Crystal Data Centre (CCDC 1016556).

■ AUTHOR INFORMATION

Corresponding Authors

*E-mail for S.T.: s-takaishi@m.tohoku.ac.jp.

*E-mail for M.Y.: yamasita@agnus.chem.tohoku.ac.jp.

Present Address

[∇]Research Institute of Instrumentation Frontier, National Institute of Advanced Industrial Science and Technology (AIST), Ibaraki 305-8568, Japan.

Author Contributions

All authors contributed to the preparation of this manuscript. All authors have given approval to the final version of the manuscript.

Notes

The authors declare no competing financial interest.

■ ACKNOWLEDGMENTS

This work was partially supported by a JSPS KAKENHI Grant (A) 26248015 and by a Grant-in-Aid for Young Scientist (B) 25810032.

■ REFERENCES

(1) (a) Tanaka, M.; Kurita, S.; Kojima, T.; Yamada, Y. *Chem. Phys.* **1984**, *91*, 257−265. (b) Wada, Y.; Mitani, T.; Yamashita, M.; Koda, T. *J. Phys. Soc. Jpn.* **1985**, *54*, 3143−3153.

(2) (a) Clark, R. J. H.; Franks, M. L.; Trumble, W. R. *Chem. Phys. Lett.* **1976**, *41*, 287−292. (b) Clark, R. J. H.; Kurmoo, M.; Mountney, D. N.; Toftlund, H. *J. Chem. Soc., Dalton Trans.* **1982**, *9*, 1851−1860. (c) Clark, R. J. H. *Chem. Soc. Rev.* **1990**, *19*, 107−131.

(3) Tanino, H.; Kobayashi, K. *J. Phys. Soc. Jpn.* **1983**, *52*, 1446−1456.

(4) (a) Iwasa, Y.; Funatsu, E.; Hasegawa, T.; Koda, T.; Yamashita, M. *Appl. Phys. Lett.* **1991**, *59*, 2219−2221. (b) Kishida, H.; Matsuzaki, H.; Okamoto, H.; Manabe, T.; Yamashita, M.; Taguchi, Y.; Tokura, Y. *Nature* **2000**, *405*, 929−932.

(5) Takaishi, S.; Tobu, Y.; Kitagawa, H.; Goto, A.; Shimizu, T.; Okubo, T.; Mitani, T.; Ikeda, R. *J. Am. Chem. Soc.* **2004**, *126*, 1614−1615.

(6) (a) Nasu, K. *J. Phys. Soc. Jpn.* **1984**, *52*, 3865−3873. (b) Webber-Milbrodt, S. M.; Gammel, J. T.; Bishop, A. R., Jr. *Phys. Rev. B* **1992**, *45*, 6435−6458. (c) Iwano, K.; Nasu, K. *J. Phys. Soc. Jpn.* **1992**, *61*, 1380−1389.

(7) Okamoto, H.; Shimada, Y.; Oka, Y.; Chainani, A.; Takahashi, T.; Kitagawa, H.; Mitani, T.; Toriumi, K.; Inoue, K.; Manabe, T.; Yamashita, M. *Phys. Rev. B* **1996**, *54*, 8438−8445.

(8) Robin, M. B.; Day, P. *Adv. Inorg. Chem. Radiochem.* **1968**, *10*, 247−422.

(9) Okamoto, H.; Yamashita, M. *Bull. Chem. Soc. Jpn.* **1998**, *71*, 2023−2039.

(10) Wolffram, H. Dissertation; Königsberg, Germany, 1900.

(11) Takaishi, S.; Takamura, M.; Kajiwara, T.; Miyasaka, H.; Yamashita, M.; Iwata, M.; Matsuzaki, H.; Okamoto, H.; Tanaka, H.; Kuroda, S.; Nishikawa, H.; Oshio, H.; Kato, K.; Takata, M. *J. Am. Chem. Soc.* **2008**, *130*, 12080−12084.

(12) Takata, M.; Nishibori, E.; Kato, K.; Kubota, Y.; Kuroiwa, Y.; Sakata, M. *Adv. X-ray Anal.* **2002**, *45*, 377−384.

(13) Le Bail, A.; Duroy, H.; Fourquet, J. L. *Mater. Res. Bull.* **1998**, *23*, 447−452.

(14) Roessler, D. M. *Br. J. Appl. Phys.* **1965**, *16*, 1119−1123.

(15) Scott, B.; Love, S. P.; Kanner, G. S.; Johnson, S. R.; Wilkerson, M. P.; Berkey, M.; Swanson, B. I.; Saxena, A.; Huang, X. Z.; Bishop, A. R. *J. Mol. Struct. (THEOCHEM)* **1995**, *356*, 207−229.

(16) Kimizuka, N.; Oda, N.; Kunitake, T. *Inorg. Chem.* **2000**, *39*, 2684−2689.

(17) (a) Okaniwa, K.; Okamoto, H.; Mitani, T.; Toriumi, K.; Yamashita, M. *J. Phys. Soc. Jpn.* **1991**, *60*, 997−1004. (b) Kumagai, S.; Takaishi, S.; Breedlove, B. K.; Okamoto, H.; Tanaka, H.; Kuroda, S.; Yamashita, M. *Chem. Commun.* **2014**, *50*, 8382−8384.

(18) Shannon, R. D.; Prewitt, C. T. *Acta Crystallogr., Sect. B* **1969**, *B25*, 925−946.